


ORIGINAL ARTICLE

Open Access



Discriminative Features of Abnormities in a Spiral Groove Gas Face Seal Based on Dynamic Model Considering Contact

Yuan Yin¹, Weifeng Huang^{1*} , Decai Li¹, Songtao Hu², Xiangfeng Liu¹ and Ying Liu¹

Abstract

It is a difficult task to root the cause of the failure of a gas face seal because different causes may result in similar observations. In the work being presented, the discrimination of multiple types of abnormities in a spiral groove gas face seal is studied. A dynamic model is employed to analyze groups of cases in order to uncover the dynamic behaviors when the face contact is induced by different mixtures of abnormities, whose discriminative features when motion and contact are monitored are studied and uncovered. A circumferential-pattern-related oscillation phenomenon is discovered, which is extracted from contact information and implies the relative magnitude of the moment on stator and the rotor tilt. The experimental observation shows consistent results. It means that the grooves (or other circumferential patterns) generate useful informative features for monitoring. These results provide guidance for designing a monitored gas face seal system.

Keywords: Gas face seals, Dynamics, Tribology, Nonlinear system

1 Introduction

As a kind of non-contacting mechanical face seal, gas face seals run with their relatively rotating faces separated by micro-scale gas films when working properly, and are thus expected a long service life [1]. However, errors from manufacturing, assembling, and servicing, along with perturbations of operating conditions, may result in a seal failure [1–4]. In most cases, the failure is led by the damage of the end faces when a severe friction beyond the designed level occurs [2].

In order to obtain detailed real-time information, efforts have been made to implant sensors or special measurable structures inside the mechanical face seals (including gas face seals). Researchers have realized seal ring temperature monitoring [5–8], motion or face separation monitoring [9–13], film pressure field monitoring

[8, 14], acoustic emission monitoring [15–22], etc.. However, it is still a challenging task to root the cause of the phenomena observed through the sensor(s). For example, one can find abnormal friction through an increased temperature or acoustic emission power [6, 15], but must do more to further tell the cause of the abnormal friction. Because implanting sensors involves revising the seal structure and weakening the seal performance, the type of sensors should be carefully decided.

Studies have been working on finding out the seal behavior dependence on the potential abnormities in the seal system through numerical simulation. Miller et al. [23] established a method coupling the lubrication and kinetic equations and analyzed the tracking of a flexibly mounted stator to a 20 μ rad rotor tilt. Green et al. [24] studied the coned gas seal responses to initial stator displacements. Lee et al. [25] studied the seal behavior when a 20 μ rad tilt was applied to both rings and found that tilting both rings led to slight periodic axial fluctuation, whereas tilting a single ring does not. Hu et al. [26] conducted a parametric study of the

*Correspondence: huangwf@tsinghua.edu.cn

¹ State Key Laboratory of Tribology, Tsinghua University, Beijing 100084, China

Full list of author information is available at the end of the article

secondary seal. Chen et al. [27] discussed the impact of gas film thickness disturbance of a gas face seal. Varney et al. [28] took eccentricity, rotordynamics, face contact and inertial maneuver loads into consideration, and described the calculation method for various faults including angular misalignment, eccentric rotating imbalance, and axial offset of the rotating seal element center of mass. Luo et al. [29] studied the dynamic characteristics of an upstream pumping mechanical seal under different extrusion fault degrees. He et al. [30, 31] analyzed the seal lubrication and wear under vibration loading. Jia et al. [32] analyzed the impact of the groove manufacturing error in high-speed mechanical face seal. Jin et al. [33] found that specific sealed fluid temperature may cause the two-phase mechanical seal to be unstable.

The majority of existing studies mainly focused on the respective impact of single type of abnormality, at least not providing how the combination of different types of abnormalities affects the sensor observation. However, the coexistence of multiple faults is the usual trouble in practice, which should be studied for finding out the approaches to diagnose them with specified sensor(s). Besides, the circumferential nonuniformity may also appear in the signals to imply certain modes, and will be paid attention to in the presented study.

Taking the spiral groove gas face seal as an example, the dynamic behaviors when the face contact is induced by different mixtures of common abnormalities are simulated. Considering motion monitoring and acoustic emission monitoring, which are recently regarded as of great advantage in terms of the information carried, the features for discriminating the abnormalities are analyzed in terms of how the different types of abnormalities and the seal geometrics interact.

2 Dynamic Model of Spiral Groove Gas Face Seals

The structure of the spiral groove gas face seal studied is shown in Figure 1. A stator with a planar face is flexibly mounted on a fixed seat, and a rotor with spiral grooves on the face (as shown in Figure 2) is fixed to the rotating shaft. The faces of two rings form a tribo-pair, which is full-film lubricated during normal operations.

Three degrees of freedom (DOFs) of the flexibly mounted stator are considered in such a model (see Figure 3): axial displacement z_s (which increases with separation), and tilt angles γ_{xs} and γ_{ys} around axes X and Y , respectively. The rotor face is usually not perfectly perpendicular to the shaft axis, and the tilt angle is denoted as γ_r . The motion of rotor, similarly represented by z_r , γ_{xr} and γ_{yr} , are regarded as given.

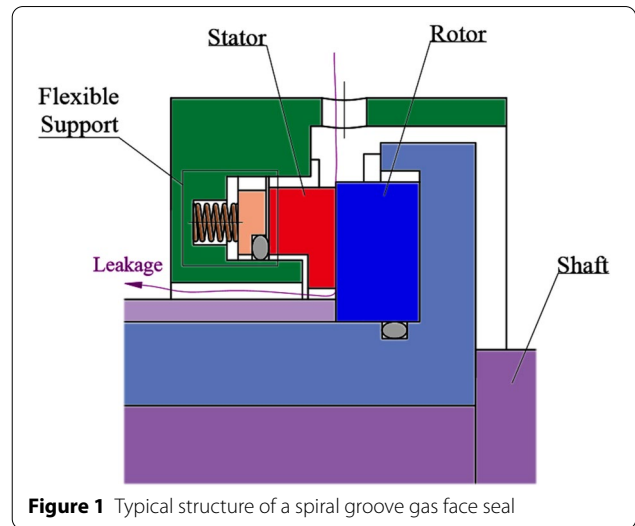


Figure 1 Typical structure of a spiral groove gas face seal

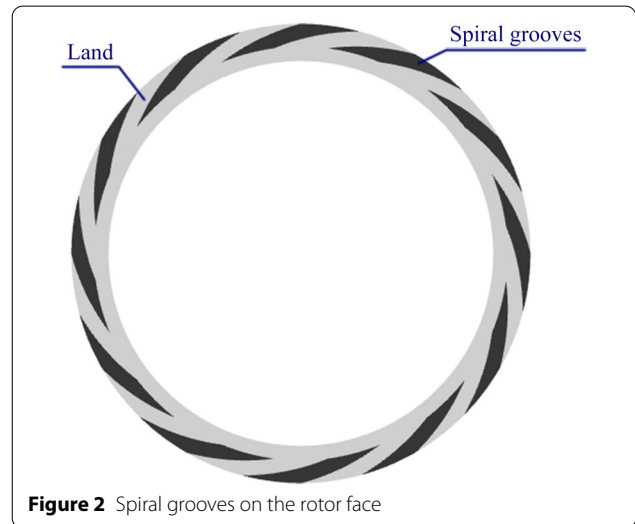


Figure 2 Spiral grooves on the rotor face

Generalized displacements are defined below:

$$\mathbf{U}_s = \begin{bmatrix} z_s \\ \gamma_{xs} \\ \gamma_{ys} \end{bmatrix}, \tag{1}$$

$$\mathbf{U}_r = \begin{bmatrix} z_r \\ \gamma_{xr} \\ \gamma_{yr} \end{bmatrix} = \begin{bmatrix} 0 \\ \gamma_r \cos \omega t \\ -\gamma_r \sin \omega t \end{bmatrix}, \tag{2}$$

$$\mathbf{U}_{Rel} = \begin{bmatrix} z_{Rel} \\ \gamma_{xRel} \\ \gamma_{yRel} \end{bmatrix} = \mathbf{U}_s - \mathbf{U}_r. \tag{3}$$

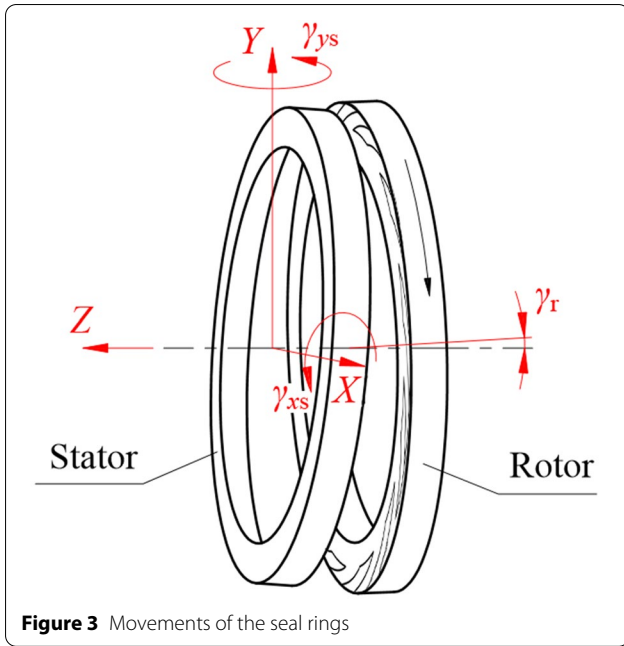


Figure 3 Movements of the seal rings

The relative generalized displacement, \mathbf{U}_{Rel} , determines the clearance distribution as:

$$h = h_0 + [1 \ y \ -x] \mathbf{U}_{\text{Rel}} + \delta h_{\text{spr}} + \frac{r - r_i}{r_o - r_i} h_{\text{coning}} \quad (4)$$

Eq. (4) is defined on an annulus area, $A = \{(x, y) | r_i \leq \sqrt{x^2 + y^2} \leq r_o\}$, which is also the domain where gas pressure and contact pressure are defined. h_{spr} is the groove depth. δ is equal to 1 in grooves, and is equal to 0 elsewhere. h_{coning} is the tap height of coning (counting the faces of both rings).

Considering the gas as ideal and inertialess with constant temperature and viscosity, and the flow as laminar flow with non-slip boundary, the absolute gas pressure in the film, p , is governed by the average flow Reynolds equation [34]:

$$\nabla \cdot \left(\frac{\varphi p h^3}{12\mu} \nabla p \right) = \frac{\omega \partial(p h)}{2\partial\theta} + \frac{\partial(p h)}{\partial t}, \quad (5)$$

$$\begin{cases} p|_{r=r_i} = p_i, \\ p|_{r=r_o} = p_o, \end{cases} \quad (6)$$

where t is the time, r and θ are the radius and angle in polar coordinates, respectively, and μ is the gas dynamic viscosity. φ is the flow factor calculated as Eq. (7) [[34]].

$$\varphi = 1 - 0.9 \exp\left(-0.56 \frac{h}{\sigma}\right). \quad (7)$$

The transient leakage can be calculated as

$$q = \oint_{\Gamma_i} \left(-\frac{\varphi p h^3}{12\mu} \nabla p \cdot \mathbf{n} dl \right) / p_a, \quad (8)$$

where Γ_i is the circle of the inner radius. In practice, only the average leakage makes sense.

The contact is simulated with a Chang-Etsion-Bogy (CEB) contact model. The contact is represented with a pressure, p_c , depending on local clearance, h , as Eqs. (9) and (10) [35].

$$\begin{aligned} p_c &= p_c(h) \\ &= \frac{4}{3} E \eta_s R_s^{\frac{1}{2}} \int_h^{h+\omega_c} \frac{(w-h)^{\frac{3}{2}}}{\sigma_s} \phi\left(\frac{w-\bar{w}_s}{\sigma_s}\right) dw \\ &\quad + \pi \eta_s R_s p_m \int_{h+\omega_c}^{\infty} \frac{2(w-h) - \omega_c}{\sigma_s} \phi\left(\frac{w-\bar{w}_s}{\sigma_s}\right) dw. \end{aligned} \quad (9)$$

$$\omega_c = \left(\frac{\pi p_m}{2E} \right)^2 R_s, \quad (10)$$

where, the mated faces are treated as an ideal rigid smooth surface and an equivalent rough surface with the parameters below: E is Young's modulus, η_s is the asperity density, R_s is the average radius of asperity tips, σ_s is the standard deviation of asperity height, \bar{w}_s is the mean of asperity height beyond the nominal plane, ω_c is the critical interference at which the plastic deformation initiates, and p_m is the maximum contact pressure. $\phi(\cdot)$ represents the probability density function of the standard normal distribution.

The support through the springs and secondary seal is modeled as providing linear stiffness and damping [[23], 35, 36]. Therefore, the stator movement is governed by:

$$\mathbf{M} \ddot{\mathbf{U}}_s + \mathbf{C}_s \dot{\mathbf{U}}_s + \mathbf{K}_s \mathbf{U}_s = \mathbf{Q} + \mathbf{P}, \quad (11)$$

where, $\mathbf{M} = \text{diag}(m, J, J)$, $\mathbf{C}_s = \text{diag}(c_{zs}, c_{\gamma_s}, c_{\gamma_s})$, and $\mathbf{K}_s = \text{diag}(k_{zs}, k_{\gamma_s}, k_{\gamma_s})$. The generalized force, \mathbf{Q} , includes the force from the tribo-pair (gas film and contact) and a counterbalance which makes $\mathbf{Q} = 0$ when $\mathbf{U} = 0$. \mathbf{P} is composed with the factors concerned which act as force or moment.

$$\mathbf{Q} = \begin{bmatrix} \iint_A (p + p_c) dA - F_{\text{eq}} \\ \iint_A (p + p_c) y dA \\ - \iint_A (p + p_c) x dA \end{bmatrix}, \quad (12)$$

$$P = \begin{bmatrix} F_z \\ M_x \\ 0 \end{bmatrix}. \tag{13}$$

The system with lubrication, contact, and kinetics coupled was solved by calculating Eqs. (1) to (13) using finite element method. The geometry was meshed into 1344 quadrilateral elements with quadratic Lagrange shape function. A stationary solve of p is first obtained

Table 1 Parameters of the gas face seal

Parameters	Values
Outer radius r_o (mm)	61.6
Inner radius r_i (mm)	51.6
Spiral groove inner radius r_{spr} (mm)	55.5
Spiral groove angle β_{spr} (°)	15
Groove depth h_{spr} (μ m)	6
Groove count N_{spr}	12
Stator mass m (kg)	0.2
Stator moment of inertia J ($kg \cdot m^2$)	3.5×10^{-4}
Support axial stiffness k_{z50} (N/m)*	1.64×10^4
Support angular stiffness k_{y50} ($N \cdot m/rad$)*	31
Support axial damping c_{z50} ($N \cdot s/m$)*	1×10^3
Support angular damping c_{y50} ($N \cdot m \cdot s/rad$)*	1.4
Standard deviation of surface height σ_a (μ m)	0.177
Standard deviation of asperity height σ_s (μ m)	0.170
Mean of asperity height \bar{w}_s (μ m)	0.114
Asperity density η_s (μ m $^{-2}$)	0.133
Average radius of asperity tips R_s (μ m)	3.02
Young's Modulus E (GPa)	151
Maximum contact pressure p_m (MPa)	242.24
Gas dynamic viscosity μ (Pa · s)	1.8×10^{-5}
Gas density under 0.1MPa ρ (kg/m^3)	1.2
Absolute gas pressure at inner radius p_i (MPa)	0.1
Absolute gas pressure at outer radius p_o (MPa)	0.5
Land clearance at zero displacement h_0 (μ m)	1.93
Rotation speed n_ω (r/min)	1200

*The marked properties are scaled as a type of abnormality in the cases simulated.

at $U_{Rel} = 0$. Then, a transient calculation is conducted, with the abovementioned stationary solve as the initial value of p and a perfect tracing status as the initial value of kinetic variants. The parameters are listed in Table 1.

3 Effects of Mixed Abnormalities

3.1 The Moment on Stator and the Rotor Tilt with Different Relative Magnitudes

Rotor tilt, represented by γ_r , exists widely in seals and was studied here. In normal cases, this affects the seal little thanks to the well-designed tracing mechanism, while a usual situation is that the flexible support performs worse than expected, represented as a factor Q_s scaling the support stiffness and damping.

Another common problem is the circumferential asymmetry of the stator and its supports [[10]], modelled with a moment around axis X , M_x , exerted on the stator.

With the support parameters scaled to $Q_s = 10$ times, a 7.2 N·m moment on the stator and a 4 mrad tilt on the rotor were mixed with varying weights (see Table 2), and the dynamic responses to the mixtures were calculated. Axial force F_z and tap height h_{coning} are not considered. These cases will be referred to as Group 1.

The results of Group 1 are listed in the last two columns of Table 2 and illustrated in Figure 4. The figure includes the three dimensions of the generalized stator displacement and the contact force, along with frequency spectrums obtained by Fourier transform exhibiting their oscillation components. Three aspects of phenomena are uncovered from the results:

- 1) Strong tracing. The motion of the stator is very close to that of the rotor (as long as the latter exists).
- 2) Fluctuations on shaft revolution period. The amplitudes of two angular stator DOFs increased with rotor tilt due to tracing. As for axial displacement and contact forces, neither isolated M_x nor γ_r led to fluctuation on the period of shaft revolution, but their combination did. Besides, the coexistence of M_x and γ_r leads to smaller leakage.

Table 2 Group 1: Mixtures of the moment on stator and the rotor tilt with varying weights

Case number	M_x (N · m)	γ_r (mrad)	Angular amplitude (mrad)	Leakage (sL/min)
1-1	7.2	0	0.0520	0.632
1-2	$6.3 = 7.2 \times 7/8$	$0.5 = 4 \times 1/8$	0.4988	0.507
1-3	$5.4 = 7.2 \times 3/4$	$1 = 4 \times 1/4$	0.9981	0.436
1-4	$3.6 = 7.2 \times 1/2$	$2 = 4 \times 1/2$	1.9961	0.390
1-5	$1.8 = 7.2 \times 1/4$	$3 = 4 \times 3/4$	2.9933	0.428
1-6	$0.9 = 7.2 \times 1/8$	$3.5 = 4 \times 7/8$	3.4913	0.491
1-7	0	4	3.9906	0.613

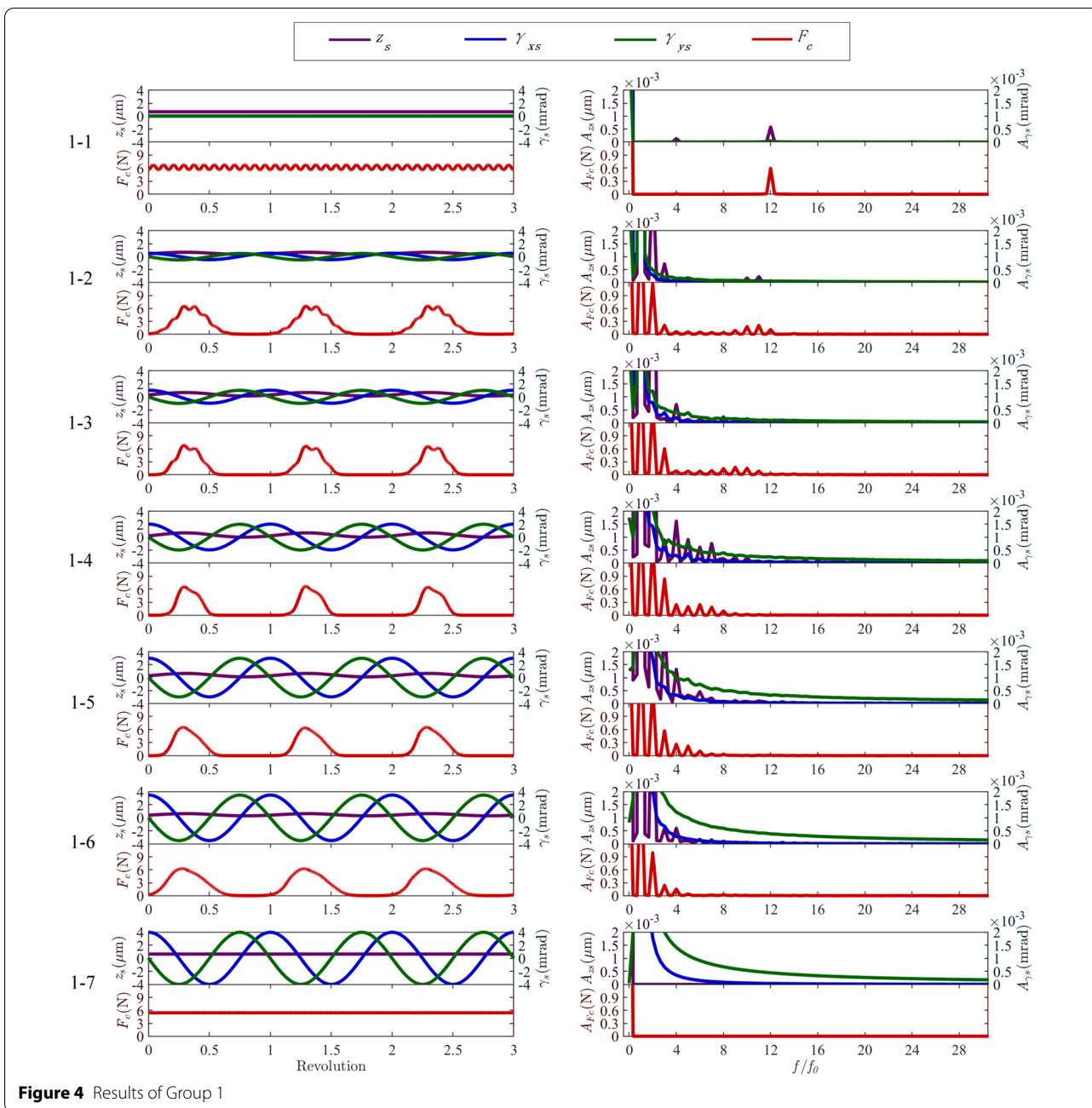


Figure 4 Results of Group 1

3) Circumferential-pattern-related oscillation. In Case 1-1, M_x induced a 12th harmonic in motion and contact (particularly distinct in contact), which corresponded to the 12 spiral grooves on the rotor face. This was not observed in Case 1–7 where only γ_r affected the seal. Similar oscillations existed in other cases but were dispersed into multiple harmonics

and could be intuitively described as shifting left with increasing rotor tilt weight. Such harmonics will be referred to as “circumferential-pattern-related oscillation” for brevity in this work. Though similar appearance of harmonics has been adopted as significant informative features in the field of bearings [37, 38], the phenomenon of dispersing and shifting found

here has not been noticed in the existing research of mechanical seals, and will be focused later.

3.2 Scaled Support Stiffness and Damping

The stator is flexibly supported by the springs and secondary seal, which inevitably suppresses the tracing behavior [23, 26]. This magnifies the impact of rotor tilt because it actually takes effect upon the seal system through tracing errors. The unexpected performance of the supports, especially the secondary seal, has been considered a significant cause of failure [1, 2, 39].

See Table 3, the scaling factor Q_s of supporting stiffness and damping were changed, forming Groups 2a (with the rotor tilt changing reciprocally) and 2b (with the rotor tilt unchanged). The results are listed in Table 3 and illustrated in Figure 5.

Although the motion of the stator is always close to that of the rotor, a greater Q_s leads to a weakening of the tracing ability, and thus magnifies the impact of rotor tilt. The abovementioned shifting of circumferential-pattern-related oscillations also show up in the results, and their ineffective in discriminating the influence of γ_r and Q_s can be uncovered by Group 2a, where a measurement for the motion of the stator is necessary.

3.3 Scaled Moment on Stator and the Rotor Tilt

In Section 3.1, cases were formed by mixing the moment on stator and the rotor tilt by weights whose sums are fixed to 1. As another dimension, Group 3 (shown in Table 4) was generated by scaling the magnitudes of M_x and γ_r based on Case 1-2. The results are listed in Table 4 and illustrated in Figure 6, showing that:

- (1) When the magnitudes scaled up, the fluctuation of generalized displacement and contact force

increased. Moreover, the scaling up increased the duration of contact in each shaft revolution, and eventually led to a continuous contact instead of an intermittent one.

- (2) However, the frequency band in which the circumferential-pattern-related oscillations distribute does not shift.

3.4 The Varying Axial Force

The axial compactness change, which may be induced by an axial size error, is modelled by a force exerted on the stator. Group 4, shown in Table 5, was generated based on Case 1-2 by adding varying axial forces F_z on the stator. The results are listed in Table 5 and illustrated in Figure 7. Besides the direct impact on leakage, the results show:

The mean of F_c changed with axial force monotonically, reaching a minimum at -50 N. This was caused by two opposing mechanisms:

- ① A force pushing the stator towards the rotor compresses them to induce contact, as a straightforward result.
- ② A force pulling the stator away from the rotor magnifies the effect of existing rotor tilt and/or moment on stator, thus aggravating contact.

This means that separating the stator with an axial force may not always alleviate or eliminate contact.

As the axial force pushed the stator towards the rotor, the amplitude of circumferential-pattern-related oscillation decreased and eventually became indiscernible. Until getting indiscernible, the circumferential-pattern-related oscillations did not shift, which demonstrated an independence from axial forces.

Table 3 Groups 2a and 2b: Changes of the supports behind the stator

Case number	M_x (N · m)	γ_r (mrad)	Q_s	Angular amplitude (mrad)	Leakage (sL/min)
2a-1	6.3	1	5	0.9985	0.507
2a-2 (1-2)	6.3	0.5	10	0.4988	0.507
2a-3	6.3	0.25	20	0.2490	0.505
2b-1	6.3	0.5	5	0.4992	0.497
2b-2(1-2)	6.3	0.5	10	0.4988	0.507
2b-3	6.3	0.5	20	0.4979	0.546

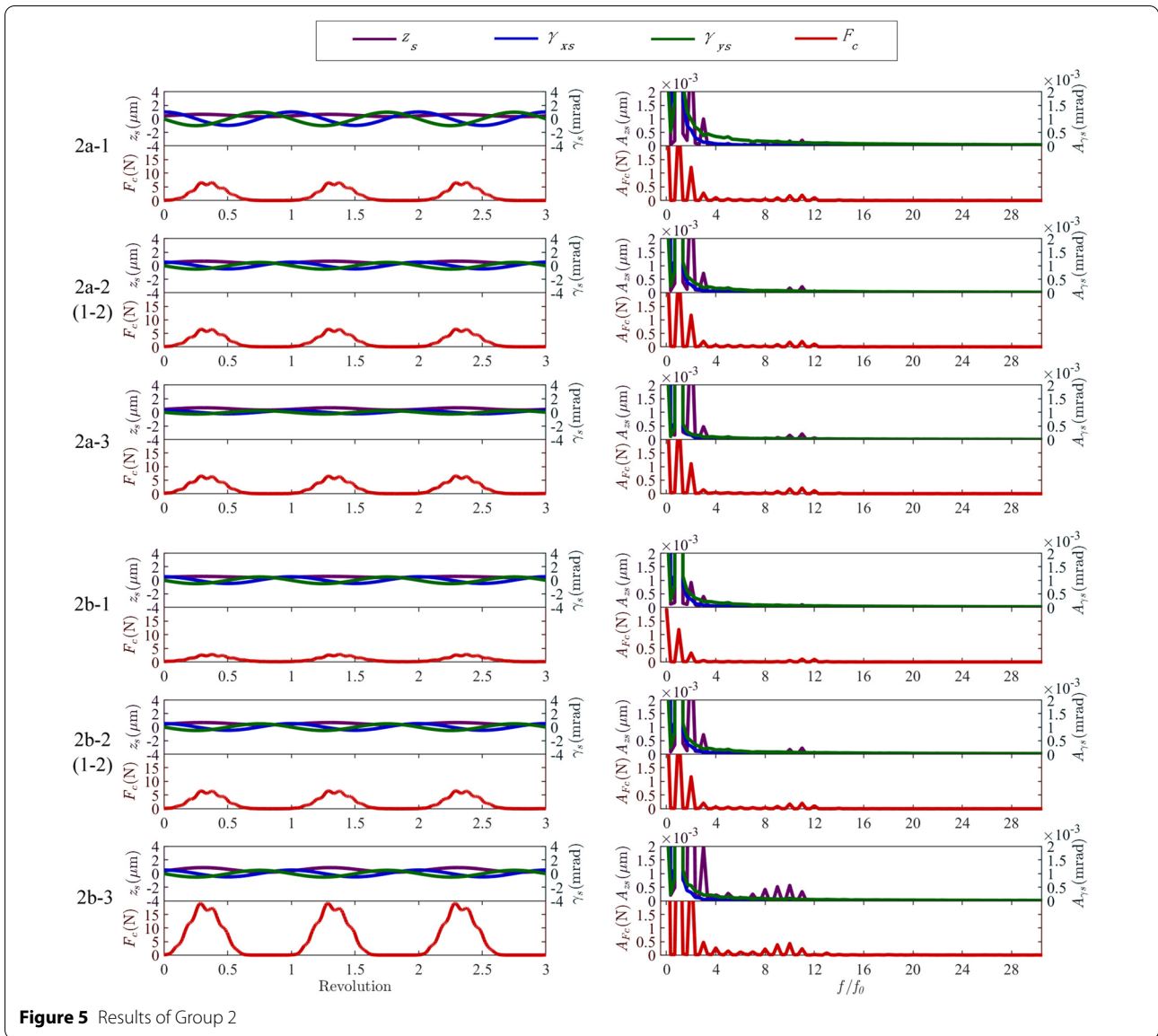


Figure 5 Results of Group 2

Table 4 Group 3: Scaling of the moment and the tilt

Case number	M_x (N · m)	γ_r (μ rad)	Angular amplitude (mrad)	Leakage (sL/min)
3-1	5.04 = 6.3 × 0.8	0.4 = 0.5 × 0.8	0.3991	0.368
3-2 (1-2)	6.3	0.5	0.4988	0.507
3-3	7.56 = 6.3 × 1.2	0.6 = 0.5 × 1.2	0.5987	0.727

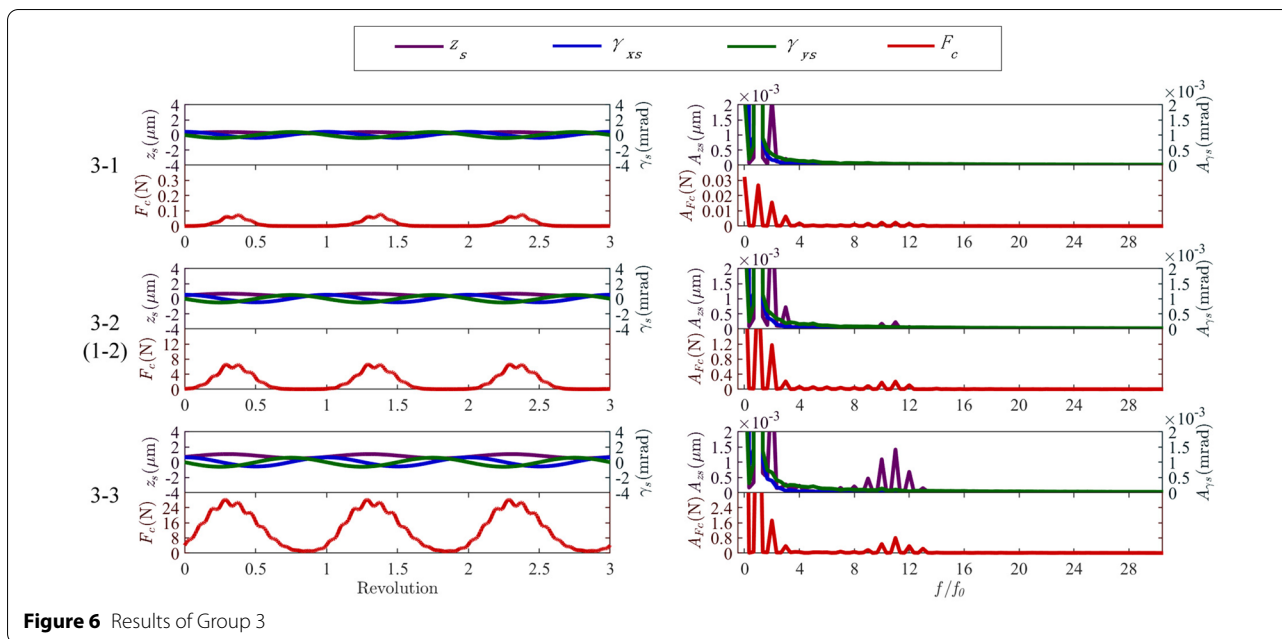


Figure 6 Results of Group 3

Table 5 Group 4: Varying axial force

Case number	M_x (N · m)	γ_r (mrad)	F_z (N)	Angular amplitude (mrad)	Leakage (sL/min)
4-1	6.3	0.5	50	0.4988	1.147
4-2 (1-2)	6.3	0.5	0	0.4988	0.507
4-3	6.3	0.5	-50	0.4990	0.287
4-4	6.3	0.5	-100	0.4992	0.184
4-5	6.3	0.5	-150	0.4996	0.127

3.5 The Varying Coning Tap Height

Coning is a common type of deformation in gas face seal, and directly affects the hydrostatic effect of the seal. Group 5 was generated based on Case 1-2 by adding varying coning tap height h_{coning} , as shown in Table 6. The results are listed in Table 6 and illustrated in Figure 8, showing that a divergent coning aggravates contact, and a convergent coning prevents contact. The coning tap height has little influence on the periodic fluctuation and harmonics.

4 Discussions

4.1 Time-frequency Domain Analysis

The results have shown that if the moment on the stator has comparative impact (compared to the tracing

error for rotor tilt) and there is not a strong pushing axial force, the high-order harmonics resulted from the spiral grooves would take place. One of their important characteristic is that with the relative impact of the rotor tilt increases, their corresponding components on the frequency spectrum disperse and shift left, and is eventually submerged in the low-order components. Such oscillations only take up an extremely small share in the motions; however, it may be distinct enough in the fluctuation of contact force when contact takes place.

We introduced the empirical mode decomposition (EMD) and Hilbert-Huang transform (HHT) to perform a time-frequency inspection on the circumferential-pattern-related oscillations. The EMD was first applied

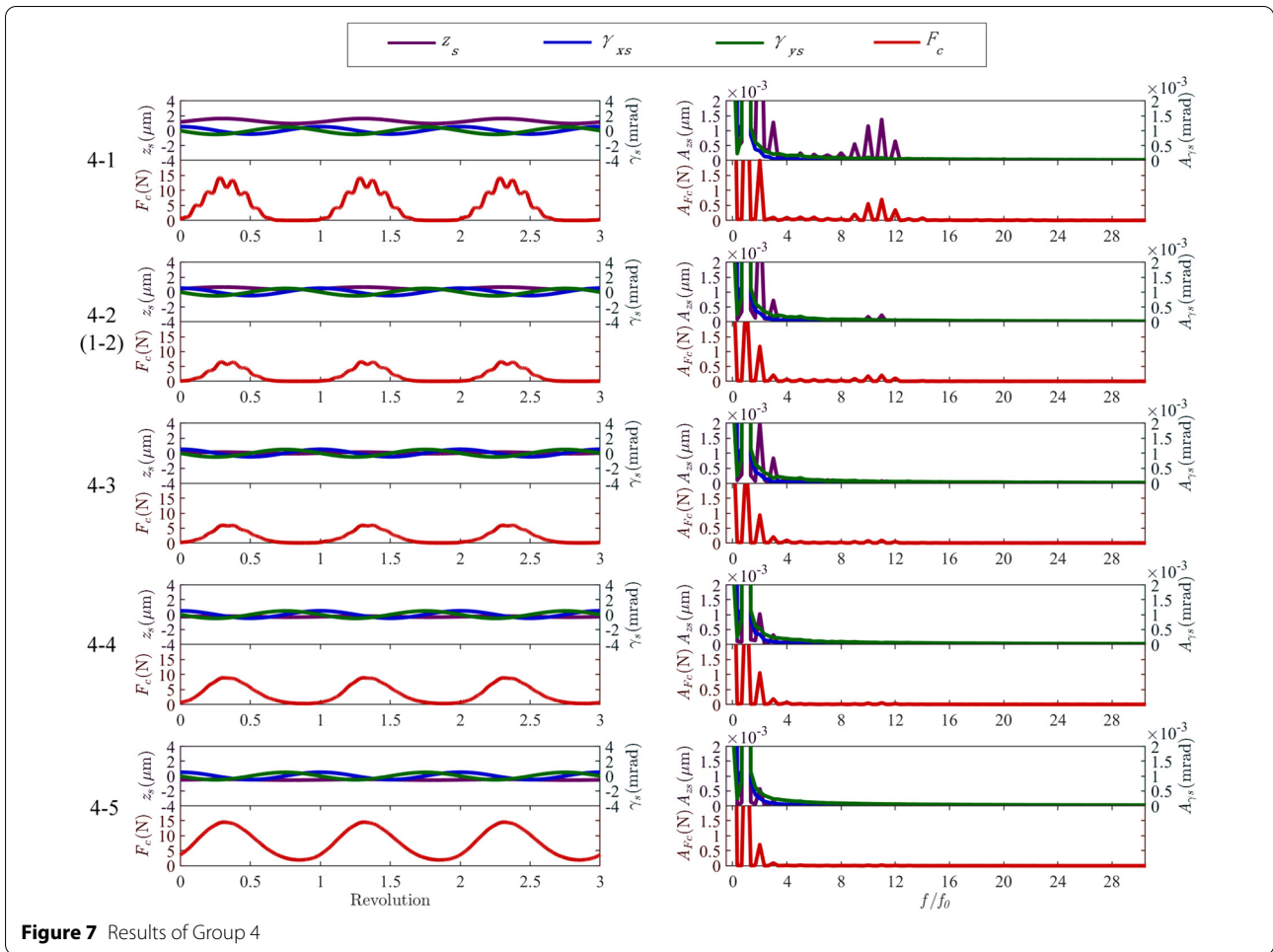
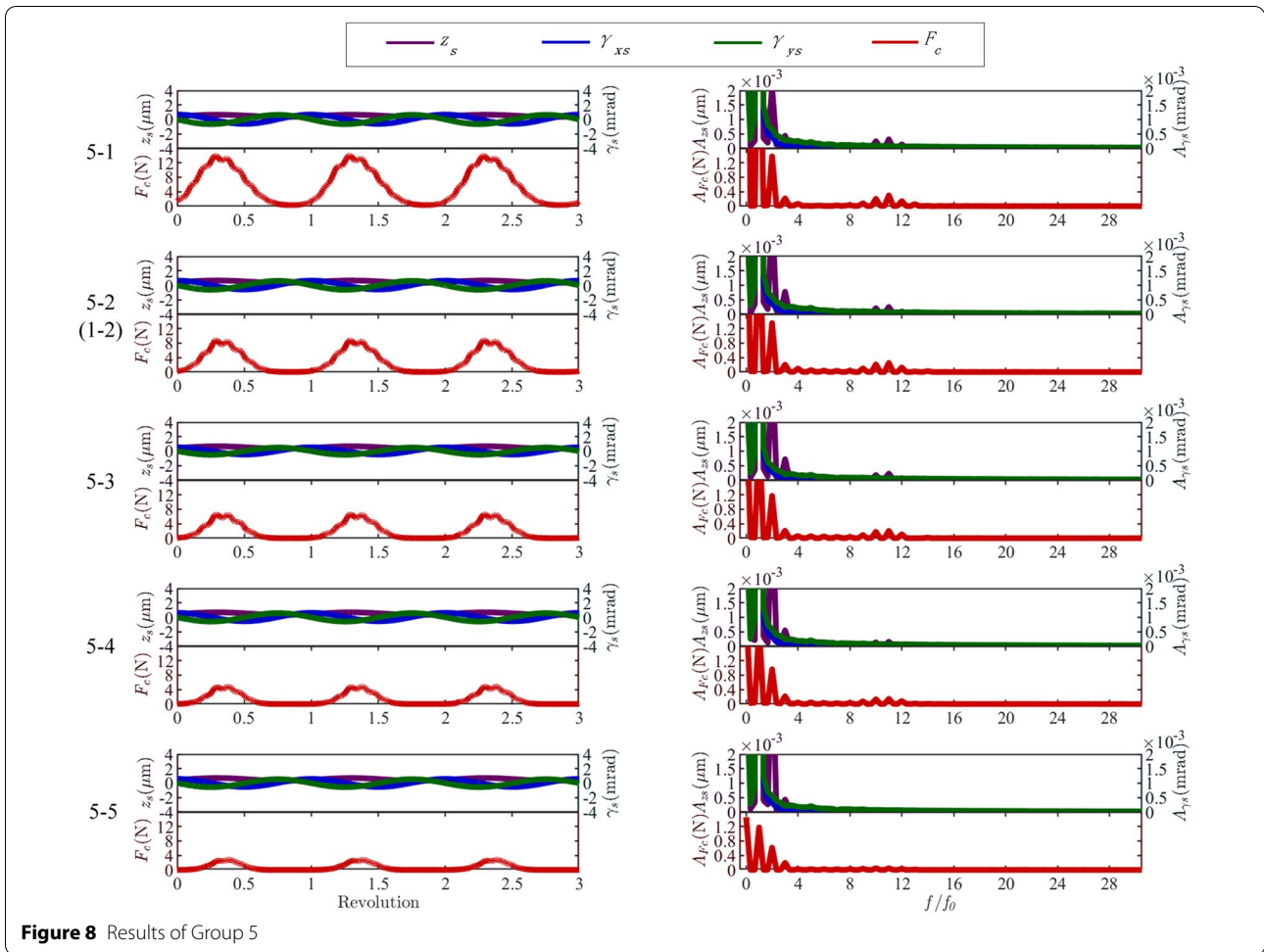


Figure 7 Results of Group 4

Table 6 Group 5: Varying coning tap height

Case number	M_x (N · m)	γ_r (mrad)	h_{coning} (μ m)	Angular amplitude (mrad)	Leakage (sL/min)
5-1	6.3	0.5	-0.3	0.6457	0.454
5-2	6.3	0.5	-0.1	0.6112	0.487
5-3 (1-2)	6.3	0.5	0	0.4988	0.507
5-4	6.3	0.5	0.1	0.5804	0.528
5-5	6.3	0.5	0.3	0.5524	0.576



to the contact forces to expose the high-order harmonics in the 1st-order intrinsic mode function (IMF), whose instant frequency were then estimated with HHT [40]. The instant frequency obtained by HHT was smoothed with a Gaussian function with a kernel of $\pi/6\omega$.

Figure 9 shows the results for Group 1 (only the first three cases) and Group 3. The abovementioned “dispersing” is actually a time-varying instant frequency, which is lower than 12th when the contact reaches maximum, and is higher than 12th in the opposite phase (as long as they are discernible). However, the oscillations are obviously weaker (Case 3-3) or even indiscernible (Cases 1-2, 1-3, 3-1 and 3-2) where they show or should have shown the

higher instant frequency. These are the reasons why the frequency distribution showed a left-shifting (compared with Case 1-1) in Figures 4 and 6, and will be referred to as a “masking” effect.

Then, the “unmasked” or intrinsic characteristic is that the instant frequency goes lower when the contact reaches maximum and goes higher in the opposite phase. As the relative impact of the rotor tilt increases, the amplitude of such fluctuation of the instant frequency goes greater.

This means that one can use such feature as an evidence in inferring the seal status: if the oscillations concentrate near the 12th harmonic, then the moment on

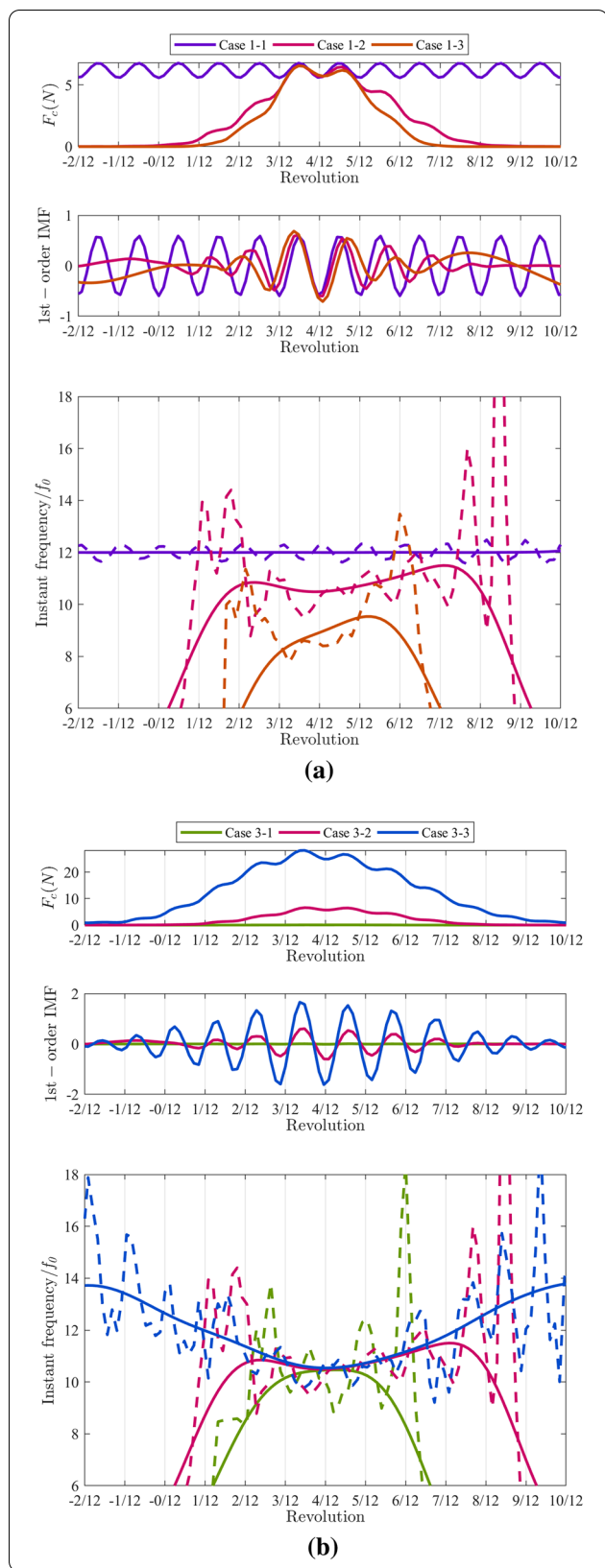


Figure 9 Time-frequency analysis. Smooth was applied on the directly generated transient frequency (by the dashed lines) to obtain the solid lines: (a) The first 3 cases in Group 1, (b) The Group 3

the stator should be the main cause; otherwise the main cause should be the rotor tilt or the stator support, but they cannot be further discriminated. The feature has enough amplitude for being recognized only in the contact force, but the contact force cannot be directly measured, so the related measurable objects such as torque and acoustic emissions should be considered, and enough frequency-domain resolution should be ensured.

4.2 Generalization for More Face Designs

Although the simulations were performed with a spiral groove face seal with 12 grooves, the mechanisms of the phenomenon and regulations found do not rely on the specific groove count or type. Here, the analysis of two cases with different face designs as illustrated in Figure 10 are presented, one with 15 grooves instead of 12 and one using T-shape grooves.

The results are shown in Figure 11.

In Case 6-1, where the groove count is 15, the abnormality parameter of Case 1-2 is used. The contact is intermittent, and the circumferential-pattern-related oscillation still exists near 13th harmonic, which can be explained by the abovementioned dispersing (around 15th harmonic) and masking (higher harmonics masked due to intermittent contact) effects.

In Case 6-2, the 12 grooves are substituted with T-shape grooves (9 μm depth in the center region and 6 μm depth in the wings). Because their hydrodynamic effect is weaker than that of the spiral grooves, M_x and γ_r are halved to $M_x = 6.3 \text{ N} \cdot \text{m} \times 0.5 = 3.15 \text{ N} \cdot \text{m}$ and $\gamma_r = 0.5 \text{ mrad} \times 0.5 = 0.25 \text{ mrad}$. The harmonics are similar with those in Case 3-3 where contact is continuous.

Therefore, it is demonstrated that the phenomenon and regulations found is general for multiple face designs.

4.3 Experimental Observations

Experiments were conducted to study the seal behaviors in abnormal conditions [15]. The test rig is of a double-face structure, where the rotor is matched with two stators with its two working faces. Only the outer tribol-pair was controlled and monitored.

In order to induce face contact against the resistance of gas film stiffness, a load mechanism was appended to the stator, as shown in Figure 12, which exerted a combination of F_z and M_x when weights were loaded, as listed in

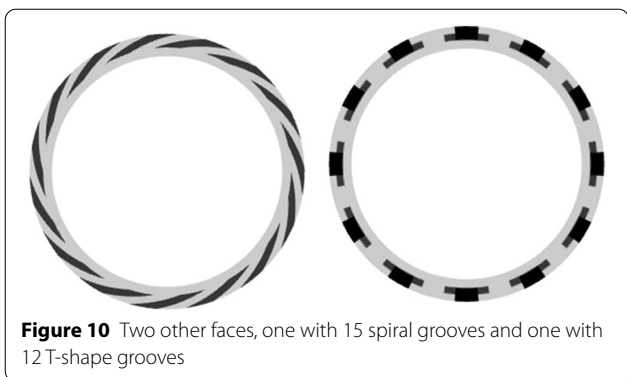


Table 7. With rotation speed and pressure fixed at 1200 r/min and 3 atmG, respectively, the mass of weights loaded varied from 1 kg to 4 kg.

The face contact was monitored by acoustic emission (AE) sensors; the signals from the one which was directly mounted to the stator were used. The short-time root-mean-square (RMS) of the high-pass filtered AE signals was calculated to represent the instant contact strength, and then processed with Fourier transform to extract the oscillation components, similar to what was performed with the simulated results in Section 3.

The results are shown in Figure 13. With the increase of loads, the spectrum tends to shift and concentrate on

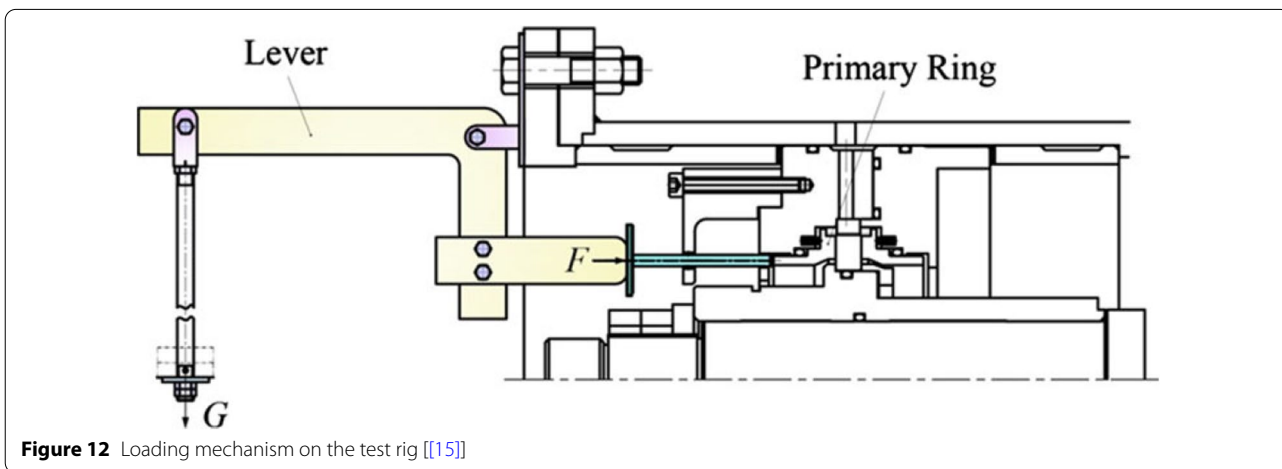
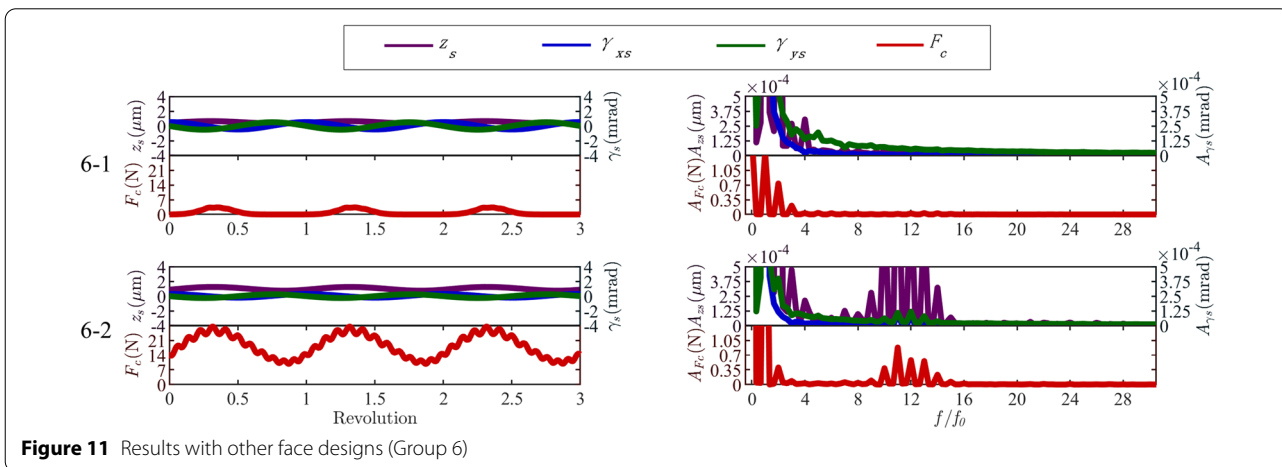


Table 7 The force and moment exerted by the load mechanism

Mass of the weights loaded (kg)	F_z (N)	M_x (N · m)
1	-29.7	1.51
2	-54.6	2.78
3	-79.5	4.05
4	-104.4	5.32

the 12th oscillation. This is because that there was an increasing M_x , while the rotor tilt γ_r brought by uncontrolled manufacturing and assembling errors remained fixed. Therefore, the regulations found by simulation are consistent with experimental observation.

5 Conclusions

The discrimination of common abnormalities in a spiral groove gas face seal is studied through numerical simulation. A dynamic model for spiral groove gas face seal

with contact considered is employed to simulate groups of cases in order to uncover the discriminative features of types of abnormalities, including the rotor tilt, the moment and force on the stator, the scaling of flexible support stiffness/damping, and the coning tap height. Conclusions are drawn as below:

- 1) The relative motion between the stator and the rotor takes only a small share compared to their absolute magnitude and is thus submerged when the latter is monitored. More information can be afforded by contact, which is necessary for discriminating the cases where the rotor tilt is at the same value but the state of the stator flexible support differs.
- 2) A phenomenon of circumferential-pattern-related oscillation is newly found, and is demonstrated by experimental observation. Only in the dynamic contact information may it be discernible. It exhibits fluctuating instant frequency, which intrinsically goes lower when the contact force reaches maximum and

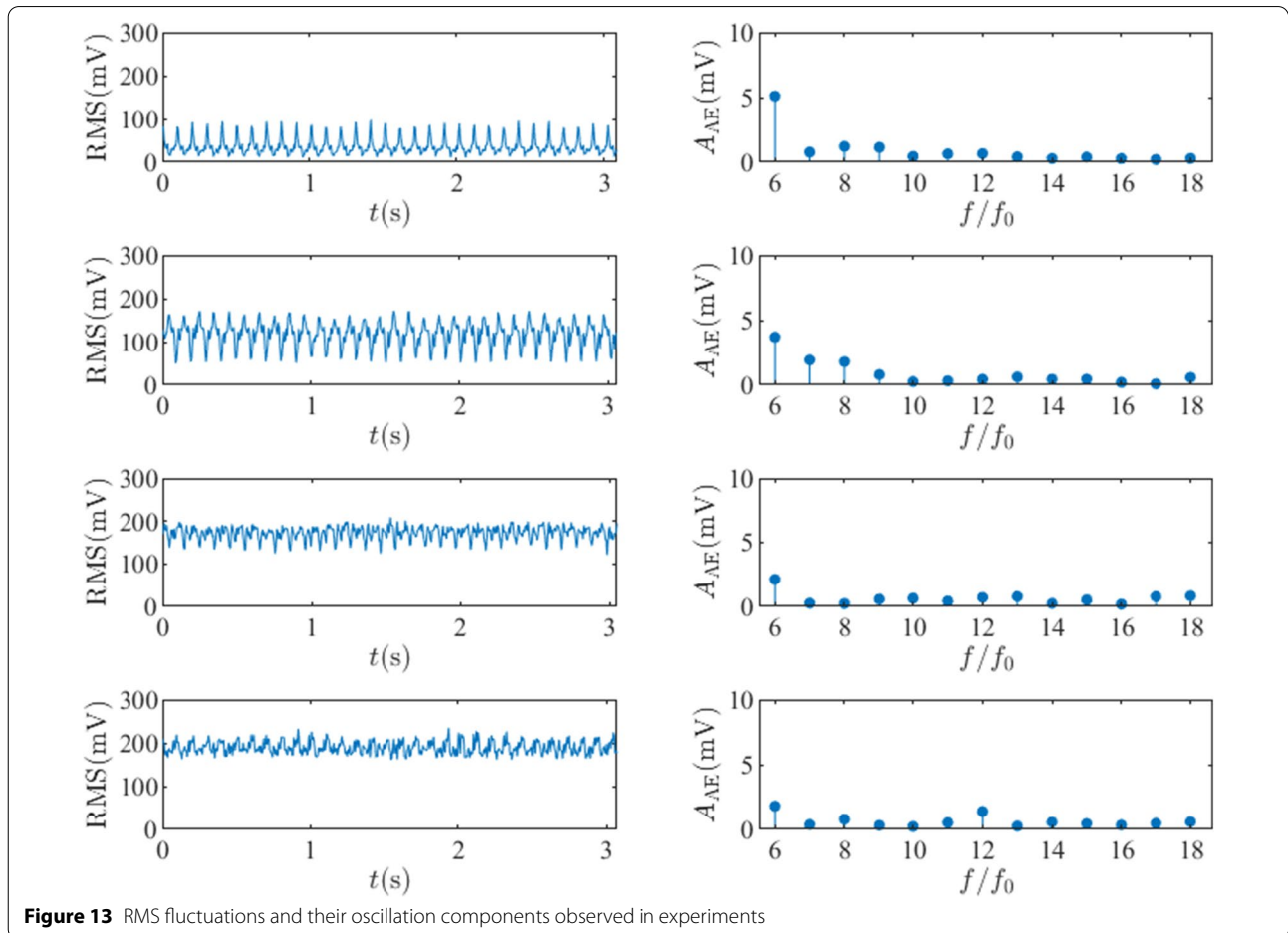


Figure 13 RMS fluctuations and their oscillation components observed in experiments

goes higher in the opposite phase, the latter of which may be “masked” by the contact intermittence. This means that the grooves (or other circumferential patterns) can be helpful in monitoring or even intentionally designed for it.

Acknowledgements

Not applicable.

Authors' contributions

YY performed the simulations and wrote the manuscript. WH and SH provided the numerical model and program. DL provided guidance on the design of cases. XL and YL modified the manuscript to improve the presentation. All authors read and approved the final manuscript.

Authors' Information

Yuan Yin, born in 1993, is currently a postdoctoral researcher at State Key Laboratory of Tribology, Tsinghua University, China. His research mainly focus on the modelling and monitoring for mechanical face seals.

Weifeng Huang, born in 1978, is currently an associate professor at State Key Laboratory of Tribology, Tsinghua University, China.

Decai Li, born in 1965, is currently a professor at State Key Laboratory of Tribology, Tsinghua University, China.

Songtao Hu, born in 1989, is currently an associate professor at State Key Laboratory of Mechanical System and Vibration, Shanghai Jiao Tong University, China.

Xiangfeng Liu, born in 1961, is currently a professor at State Key Laboratory of Tribology, Tsinghua University, China.

Ying Liu, born in 1965, is currently an associate professor at State Key Laboratory of Tribology, Tsinghua University, China.

Funding

Supported by the National Key R&D Program of China (Grant No. 2020YFB2010000) and the National Natural Science Foundation of China (Grant No. U1737209).

Competing interests

The authors declare no competing financial interests.

Author Details

¹State Key Laboratory of Tribology, Tsinghua University, Beijing 100084, China.

²State Key Laboratory of Mechanical System and Vibration, Shanghai Jiao Tong University, Shanghai 200240, China.

Received: 12 January 2021 Revised: 27 December 2021 Accepted: 18 February 2022

Published online: 17 March 2022

References

- [1] B S Nau. Rotary mechanical seals in process duties: An assessment of the state of the art. *Proceedings of the Institution of Mechanical Engineers, Part A: Journal of Power and Energy*, 1985, 199(1): 17–31.
- [2] Y E Fan, F S Gu, A D Ball. A review of the condition monitoring of mechanical seal. *Proceedings of ESDA04, 7th Biennial Conference on Engineering Systems Design and Analysis*, 2004.
- [3] S Y Ding, F C Li, Y L Wang. Research on operation and maintenance method of mechanical seals based on fault and failure analysis. *Fluid Machinery*, 2020, 48(3): 27–31. (in Chinese)
- [4] W J Zhao, J Jin, X K Meng, et al. State of the art and development trend of mechanical seal for marine equipment. *Tribology*, 2016, 39(6): 792–802. (in Chinese)
- [5] B Tournerie, D Reungent, J Frene. Temperature measurements by infrared thermography in the interface of a radial face seal. *Journal of Tribology*, 1991, 113(3): 571–576.
- [6] R L Philips, L E Jacobs. Experimental determination of the thermal characteristics of a mechanical seal and its operating environment. *Tribology Transactions*, 1997, 40(4): 559–568
- [7] K Dingui, N Brunetiere, J Bouyer, et al. Surface texturing to reduce temperature in mechanical seals. *Tribology Online*, 2020, 15(4): 222–229.
- [8] A Chavez, O D Santiago. Experimental measurements of the thermo elastic behavior of a dry gas seal operating with logarithmic spiral grooves of 11° and 15°. *Proceedings of the Institution of Mechanical Engineers, Part J: Journal of Engineering Tribology*, 2021, 235(9): 1807–1819.
- [9] E DiRusso. Film Thickness measurement for spiral groove and Rayleigh step lift pad self-acting face seals. *NASA TP-2058*, 1982.
- [10] I Etsion, I Constantinescu. Experimental observation of the dynamic behavior of noncontacting coned-face mechanical seals. *ASLE Transactions*, 1984, 27(3): 263–270.
- [11] W Anderson, J Jarzynski, R F Salant. Condition monitoring of mechanical seals: detection of film collapse using reflected ultrasonic waves. *Proceedings of the Institution of Mechanical Engineers*, 2000, 214(9): 1187–1194.
- [12] J L Wang, X H Wang, C Zhang, et al. Distribution detection method of film thickness in mechanical seal based on ultrasonic principle. *China Mechanical Engineering*, 2019, 30(6): 684–689. (in Chinese)
- [13] J J Lu. Theoretical analysis and experiment on gas film stiffness with slip flow in a spiral-grooved dry gas seal. *Industrial Lubrication and Tribology*, 2021, 73(10): 1226–1236.
- [14] J J Luo, D Brillert. Experimental investigations on the pressure fluctuations in the sealing gap of dry gas seals with embedded pressure sensors. *Journal of Engineering for Gas Turbines and Power—Transactions of the ASME*, 2021, 143(3): 031005.
- [15] W F Huang, Y B Lin, Y Liu, et al. Face rub-impact monitoring of a dry gas seal using acoustic emission. *Tribology Letters*, 2013, 52(2): 253–259.
- [16] H Towsyfyan. Investigation of the nonlinear tribological behavior of mechanical seals for online condition monitoring. Huddersfield: University of Huddersfield, 2017.
- [17] Y Yin, W F Huang, X F Liu, et al. Analysis of the dynamic friction of a gas face seal based on acoustic emissions. *Tribology Letters*, 2018, 66(3): 85.
- [18] H Towsyfyan, F S Gu, A D Ball, et al. Modelling acoustic emissions generated by tribological behaviour of mechanical seals for condition monitoring and fault detection. *Tribology International*, 2018, 125: 46–58.
- [19] Y Yin, W F Huang, X F Liu, et al. Adaptive analysis for acoustic emissions generated from a gas face seal. *IEEE Annual International Conference on Cyber Technology in Automation Control and Intelligent Systems*, 2019: 65–69.
- [20] H Towsyfyan, F S Gu, A D Ball, et al. Tribological behaviour diagnostic and fault detection of mechanical seals based on acoustic emission measurements. *Friction*, 2019, 7: 572–586.
- [21] A Daraz A, S Alabied, D Zhen, et al. Detection and diagnosis of mechanical seal faults in centrifugal pumps based on acoustic measurement. *Advances in Asset Management and Condition Monitoring*, 2020, 166: 963–975.
- [22] M Medina-Arenas M, F Sopp, J Stolle, et al. Measurement and analysis of inadequate friction mechanisms in liquid-buffered mechanical seals utilizing acoustic emission technique. *Vibration*, 2021, 4: 263–283.
- [23] B A Miller, I Green. Numerical formulation for the dynamic analysis of spiral-grooved gas face seal. *Journal of Tribology*, 2001, 123(2): 395–403.
- [24] I Green, R M Barnsby. A simultaneous numerical solution for the lubrication and dynamic stability of noncontacting gas face seals. *Journal of Tribology*, 2001, 123(2): 388–394.
- [25] S C Lee, X L Zheng. Analyses of both steady behavior and dynamic tracking of non-contacting spiral-grooved gas face seals. *Computers and Fluids*, 2013, 88(12): 326–333.
- [26] S T Hu, W F Huang, X F Liu, et al. Influence analysis of secondary O-ring seals in dynamic behavior of spiral groove gas face seals. *Chinese Journal of Mechanical Engineering*, 2016, 29(3): 507–514.
- [27] Y Chen, J B Jiang, X D Peng. Gas film disturbance characteristics analysis of high-speed and high-pressure dry gas seal. *Chinese Journal of Mechanical Engineering*, 2016, 29(6): 1226–1233.
- [28] P Varney, I Green. Dynamic modeling of an eccentric face seal including coupled rotordynamics, face contact, and inertial maneuver loads. *Proceedings of the Institution of Mechanical Engineers, Part J: Journal of Engineering Tribology*, 2018, 232: 732–748.
- [29] Y Luo, Y K Fan, Y J Han, et al. Research on the dynamic characteristics of mechanical seal under different extrusion fault degrees. *Processes*, 2020, 8: 1057.

- [30] W T He, S P Wang, C Zhang, et al. A wear simulation method for mechanical face seals under friction instability conditions. *Applied Sciences*, 2020, 10(8): 2875.
- [31] W T He, S P Wang, C Zhang, et al. Lubrication and wear characteristics of mechanical face seals under random vibration loading. *Materials*, 2020, 13(6): 1285.
- [32] Q Jia, J L Wang, Z Cui, et al. Performance analysis and optimization of mechanical seal with spiral groove manufacturing error. *Journal of Xi'an Jiaotong University*, 2020, 54(11): 46–55. (in Chinese)
- [33] J Jin, X D Peng, X K Meng, et al. Analysis of stability of two-phase flow mechanical seal with spiral groove under high speeds. *Journal of the Brazilian Society of Mechanical Sciences and Engineering*, 2021, 43: 260.
- [34] Patir N, Cheng H S. An average flow model for determining effects of three-dimensional roughness on partial hydrodynamic lubrication. *Journal of Tribology*, 1978, 100(1): 12–17.
- [35] W R Chang, I Etsion, D B Bogy. An elastic-plastic model for the contact of rough surfaces. *Journal of Tribology*, 1987, 109(2): 257–263.
- [36] L S Xu, J H Wu, Y L Wang, et al. Transient response and rub-impact phenomenon of liquid lubricated non-contacting mechanical seals during external pressure fluctuation. *Journal of the Brazilian Society of Mechanical Sciences and Engineering*. 2020, 42(8): 428.
- [37] A Srivani, T Arunkumar, S DenisAshok. Fourier harmonic regression method for bearing condition monitoring using vibration measurements. *Materials Today: Proceedings*, 2018, 5: 12151–12160.
- [38] M F Wang, Z L Mo, H Y Fu, et al. Harmonic L2/L1 norm for bearing fault diagnosis. *IEEE Access*, 2019, 7: 27313–27321.
- [39] J Xu, X D Peng, S X Bai, et al. Experiment on wear behavior of high pressure gas seal faces. *Chinese Journal of Mechanical Engineering*, 2014, 27: 1287–1293.
- [40] N E Huang, S Zheng, R L Steven, et al. The empirical mode decomposition and the Hilbert spectrum for nonlinear and non-stationary time series analysis. *Proceedings of the Royal Society A-Mathematical Physical and Engineering Sciences*, 1998, 454(1971): 903–995.

Submit your manuscript to a SpringerOpen[®] journal and benefit from:

- ▶ Convenient online submission
- ▶ Rigorous peer review
- ▶ Open access: articles freely available online
- ▶ High visibility within the field
- ▶ Retaining the copyright to your article

Submit your next manuscript at ▶ [springeropen.com](https://www.springeropen.com)
